The FASEB Journal article fj.10-175653. Published online February 24, 2011.

Comparison of homology models and crystal structures of cuticle-degrading proteases from nematophagous fungi: structural basis of nematicidal activity

Lianming Liang,*[,1] Shuqun Liu,*[,1] Jinkui Yang,* Zhaohui Meng,*[,†] Liping Lei,[‡] and Keqin Zhang*[,2]

*Laboratory for Conservation and Utilization of Bioresources and Key Laboratory for Microbial Resources of the Ministry of Education, Yunnan University, Kunming, China; [†]Laboratory of Molecular Cardiology, Department of Cardiology, First Affiliated Hospital of Kunming Medical University, Kunming, China; and [‡]Tobacco Agricultural Science Institute of Yunnan Province, Yuxi, China

ABSTRACT **Cuticle-degrading proteases secreted by nematophagous fungi can degrade nematode cuticle during infection. Alkaline proteases from nematode-parasitic fungi show stronger nematicidal activity *in vitro* than neutral proteases from nematode-trapping fungi. Sequence alignment of these proteases revealed that the active-site residues were much conserved. Disulfide bridges in alkaline proteases not only contribute to the thermal stability of enzyme structure but also increase the flexibility of S1 and S4 pockets located at the substrate-binding site. Molecular electrostatic potential surfaces of these proteases change gradually from negative to positive while arranging in the order from neutral to alkaline proteases, possibly contributing to the distinct extent of substrate (nematode cuticle) attraction by proteases. The differences in flexibility of substrate-binding site and in electrostatic surface potential distribution between neutral and alkaline cuticle-degrading proteases are associated with the changes of their catalytic activities and nematicidal activities with fungal species. Our results indicate that nematode-parasitic and nematode-trapping fungi have evolved for distinct adaptation under selective pressure.—Liang, L., Liu, S., Yang, J., Meng, Z., Lei, L., Zhang, K. Comparison of homology models and crystal structures of cuticle-degrading proteases from nematophagous fungi: structural basis of nematicidal activity. *FASEB J.* 25, 000–000 (2011). www.fasebj.org**

Key Words: disulfide bridge · structural flexibility · electrostatic surface potential

In the course of fungal infection to arthropods and nematodes, extracellular enzymes, including proteases, chitinases, and collagenases, are involved in the penetration of the host barrier (1). Among these enzymes, serine proteases are considered one of the most important virulence factors during fungal infection of animal hosts (1).

In the past 2 decades, several cuticle-degrading proteases secreted by a diverse group of nematophagous and entomopathogenic fungi, such as *Arthrobotrys oligospora* (2, 3), *Pochonia chlamydosporia* (syn. *Verticillium chlamydosporium*; ref. 4), *Beauveria bassiana* (5), and *Metarhizium anisopliae* (6), have been purified and characterized. These proteases are secreted mainly during infection and classified to the subtilisin family. An *A. oligospora* mutant carrying additional copies of the *PII* gene encoding a extracellular cuticle-degrading protease was observed to develop more infection devices and to capture and kill nematodes faster than the wild-type strain (7). Another *P. chlamydosporia* protease, VCP1, with 2 different amino acids at positions 65 and 99, was related to host preference due to distinct affinity with substrate residues at the P3 position (8). These studies provide a clue that the catalytic activity and substrate specificity can be modulated by modifying the proteases *via* site-directed mutagenesis. Understanding the structural features of the proteases is a prerequisite for clarifying possible mechanisms involved in fungal virulence. The structures of 2 nematode cuticle-degrading proteases, Ver112 and PL646, have been determined by X-ray crystallography (9). As members of the peptidase S8 family, these 2 proteases are similar in both 3-dimensional structure with an identical catalytic triad and catalytic function mechanism (9). In addition, the electrostatic surface complementarity between these 2 proteases and the nematode cuticle likely facilitate the binding of the substrate to the enzymes.

There are 2 large groups of nematophagous fungi: the nematode-parasitic fungi and the nematode-trap-

[1] These authors contributed equally to this work.

[2] Correspondence: Laboratory for Conservation and Utilization of Bioresources and Key Laboratory for Microbial Resources of the Ministry of Education, Yunnan University, Kunming 650091, China. E-mail: kqzhang111@yahoo.com.cn

doi: 10.1096/fj.10-175653

This article includes supplemental data. Please visit *http://www.fasebj.org* to obtain this information.

ping fungi. Although the nematode-trapping fungi can develop certain mycelium structures called traps to attack and grip nematodes, both groups can secrete proteases to degrade nematode cuticle (1, 10). Phylogenetic analysis based on their amino acid sequences suggested that these proteases can also be divided into 2 groups (11). Although these proteases have relatively high sequence identity and share the same functional role during nematode infection, they display differential substrate specificities and catalytic activities, likely due to the subtle differences in amino acid sequences around the substrate-binding region (12). In this study, the structural models of 14 proteases from nematode-trapping fungi were modeled using a homology-modeling technique. These structural models are compared with those of proteases from nematode-parasitic fungi. Of those, 5 were previously determined by X-ray diffraction (9) or modeling (12). Moreover, 2 proteases, Ver112 and PII, as representative members of alkaline and neutral proteases, were purified from *Lecanicillium psalliotae* and *A. oligospora*, respectively; and their catalytic activity against nematode cuticle and their thermal stability were compared. The objective of this study is to identify the key structural factors that contribute to fungal virulence against nematodes.

MATERIALS AND METHODS

Organisms and growth conditions

L. psalliotae was originally isolated from field soil in Yunnan Province and had been deposited in the China General Microbiological Culture Collection Center (CGMCC1312). It was grown in a medium described previously (13). The culture was carried out in a 500-ml flask containing 200 ml of medium at 26°C and shaken at 150 rpm for 6 d on a rotary shaker.

A. oligospora was obtained from American Type Culture Collection (ATTC; Manassas, VA, USA; ATCC 24927) and cultivated under the same condition as for *L. psalliotae*.

The saprophytic nematode *Caenorhabditis elegans* was maintained as described previously (14). It was washed thoroughly with 50 mM sodium phosphate buffer (pH 7.0) before the assays.

Multiple sequence alignment and phylogenetic analysis

Extracellular infectious proteases from nematode-trapping fungi, nematode parasitic fungi, and insect parasitic fungi were selected. Sequences were retrieved from GenBank and aligned using ClustalX 2.0 (15). The signal peptides and propeptides were excluded from further analysis. Based on this alignment, phylogeny was estimated with the neighbor-joining (NJ) method of clustering in the MEGA 4.0 program (16). Bootstrap analysis was used, with 1000 replicates to test the relative support for branches produced by the NJ analysis.

Protease modeling and evaluation

Structural models of all the proteases from nematode-trapping fungi were constructed using the program Modeller (9v3; ref. 17). The procedures were the same as those described previously (12). Briefly, the target sequence was first aligned with the template sequence using a script written in-house, "alignment." Second, 20 raw models were generated from the template using an in-house script, "get-model." The insertions and deletions were generated and optimized using a loop modeling subroutine within the get-model script with a 3D_INTERPOLATION algorithm and a thorough optimization protocol (a thorough molecular dynamics (MD)/simulated annealing procedure, with MD_LEVEL set to "refine.slow"). Finally, these 20 models were clustered, and an optimized average model was generated. All the proteases were then subjected to the steepest descent energy minimization with the tolerance 100 $kJ \cdot mol^{-1} \cdot nm^{-1}$, followed by a second conjugate gradient energy minimization with the tolerance 10 $kJ \cdot mol^{-1} \cdot nm^{-1}$, using the Gromacs software package (18, 19). The overall geometrical qualities of these models were assessed using the program Procheck (20).

MD simulation

To compare the dynamic structural properties of these proteases, 5 molecules (PII, Ver112, and 3 constructed Ver112 mutants) were chosen for MD simulations. The 3 Ver112 mutants were constructed to disrupt the disulfide bridges within the structure. For example, the mutants Ver112_C124A and Ver112_C179A disrupted the disulfide bridges Cys35-Cys124 and Cys179-Cys250, respectively, and the mutant Ver112_C124_179A contained the double mutations that simultaneously disrupted these 2 disulfide bridges.

The Gromacs package (18, 19) was used for MD simulations using the Gromos96 43a1 force field. The molecules were individually solvated using the single-point-charge water molecules (21) in a cubic box with a 1.0-nm solute-wall minimum distance. After a first steepest descent energy minimization with positional restraints on the solute, 4 and 8 chloride ions were introduced by replacing water molecules at the highest electrostatic potential to compensate for the net positive charges of the Ver112 and PII systems, respectively. A second energy minimization was then performed until no significant energy change could be detected. Subsequently, the systems were simulated for 20 ps with harmonic positional restraint force on the solutes to "soak" the water molecule into the macromolecule, followed by the production MD run of 10 ns.

During MD simulations, solute, solvent, and counterions were independently coupled to a reference temperature bath at 300 or 400 K with a coupling constant τ_t of 0.1 ps (22). The pressure was maintained by weakly coupling the system to an external pressure bath at 1 atm with a coupling constant τ_p of 0.5 ps. The nonbonded pair was updated every 10 steps, and the van der Waals interaction treatment was cut off with radius 1 nm. The electrostatic interactions were treated with particle mesh Ewald with an interpolation order of 6, Fourier spacing of 0.15 nm, and Coulomb radius of 1 nm (23). The LINCS algorithm (24) was used to constrain the bond lengths to their equilibrium positions. A 2-fs time step was used for the integration of the equation of motion.

Protease activity and stability

The typical alkaline protease Ver112 from *L. psalliotae* and neutral protease PII from *A. oligospora* were purified, respectively, from the supernatant of liquid medium as described previously (2, 13). Soluble protein was determined by Coomassie dye reaction (Bio-Rad, Hercules, CA, USA) using BSA as standard. Protease activities were measured using casein as substrate and a previously described method (25).

The optimum reaction temperature and thermal stability of the 2 proteases Ver112 and PII were measured as described

previously (13). The nematicidal activities of the 2 pure proteases against *C. elegans* were bioassayed. One unit of each of the 2 proteases was incubated with nematodes (*C. elegans*) in 1 ml water at 25°C. The numbers of immobilized and total nematodes were counted using a light microscope at 8, 16, 24, 32, 40, and 48 h, respectively.

RESULTS AND DISCUSSION

Comparison of catalytic properties and nematicidal activities between Ver112 and PII

The proteases Ver112 and PII were purified from *L. psalliotae* and *A. oligospora* using gel filtration and ion exchange chromatography, respectively. Ver112 showed the highest activity at ~60°C and maintained 50% activity after incubation for 30 min at 60°C (**Fig. 1*A***). PII showed the highest activity at ~40°C, and exhibited no activity after incubation for 30 min at 60°C (Fig. 1*B*).

C. elegans (third-stage larva) was used to compare nematicidal activities between Ver112 and PII, revealing that these 2 enzymes showed significantly different nematicidal activities (**Fig. 2**). Fifty percent of the nematodes were killed after incubation with PII for 48 h, whereas 24 h was required by Ver112 to kill the same percentage of nematodes. Figure 2 also shows that for PII the nematode mortality reach a plateau after 32 h, likely caused by the low stability of PII, as described below.

Sequence alignment

The sequences of 29 proteases from 14 nematode-trapping fungi, 6 nematode-parasitic fungi, and 9 entomopathogenic fungi were aligned. (Supplemental Fig. S1). There are 63 identical amino acids shared among all these sequences. The catalytic triad Asp-His-Ser is completely conserved, indicating a strong selective pressure for the maintenance of the architecture (and subsequently the catalysis function) of this site (12, 26). In the S1 pocket of the substrate-binding site, all residues were conserved except for those located at position 286 (*E55263* numbering). Among the neutral proteases derived from nematode-trapping fungi, position 286 is a Glu, whereas in other proteases this position is occupied by an Asp. In the S4 pocket, there are more positions that are occupied by various amino acids. For example, for position 232, there are hydrophilic residues (Thr or Asn) within the neutral proteases (Thr in EF055263, AY859781, AY859780, EF113089, EF113090, X94121, AF516146′EF113088 and EF113091; Asn in EF113092 and DQ531603) but hydrophobic residues (Tyr or Leu) within the alkaline proteases (Tyr in EF094858, L29262, AJ427454, FJ009628, and AJ416695; Leu in AY692148, S71812, U16305, AY040532, and AY520814). The difference in amino acid composition of substrate pockets can lead to subtle changes in size and hydrophathic properties of these pockets, thus resulting in different substrate specificity and catalytic activity of proteases. Apart from the relatively conserved active site, there are 4 conserved cysteines that can form 2 disulfide bridges in alkaline protease.

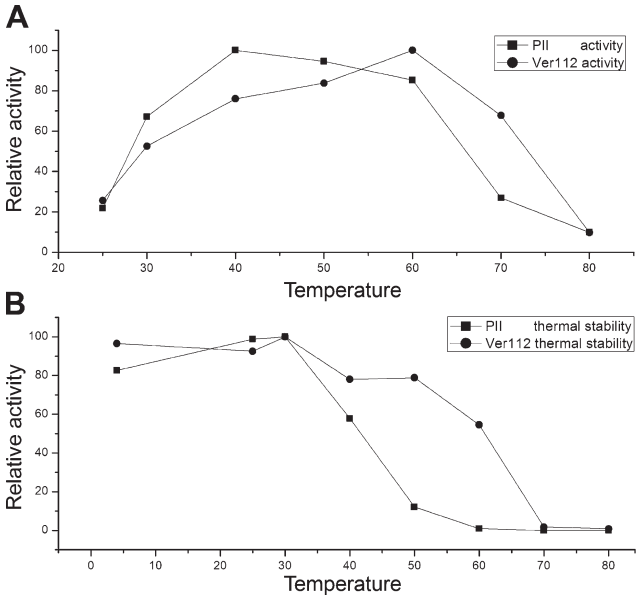

Figure 1. Effect of temperature on catalytic activity of Ver112 and PII. *A*) Purified protease Ver112 showed the highest activity at 60°C, whereas PII showed the highest activity at 40°C. *B*) Ver112 showed stronger thermal stability than PII.

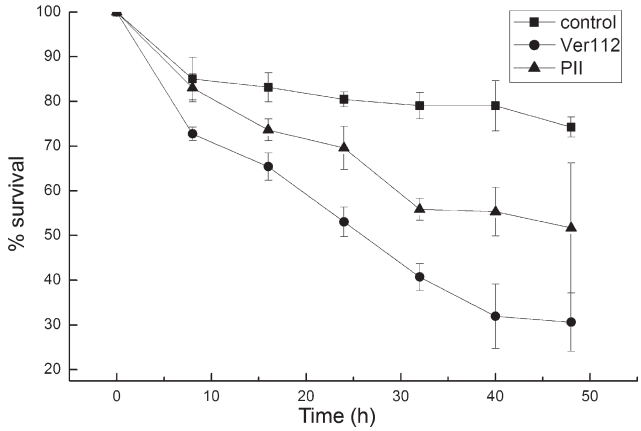

Figure 2. Kinetics of nematode survivorship in bioassays. Nematodes were suspended in protease solution of Ver112 or PII. Control nematodes were suspended in 50 mM sodium phosphate buffer at pH 7.0.

Models

To compare the structural differences between cuticle-degrading proteases from nematophagous fungi, 14 neutral proteases from nematode-trapping fungi were modeled. Alkaline proteases from nematode-parasitic fungi, including 2 crystal structures (Ver112 and PL646) and 2 previously modeled structures (PR1 and VCP1; ref. 12) were also included for comparison. These modeled structures were evaluated to have good structural qualities (**Table 1**).

TABLE 1. *Homology models of proteases from nematode-trapping fungi*

Source	Genbank ID	Procheck results: residues in regions (%)			
		Most favorite	Additionally allowed	Generously allowed	Disallowed
Micromitrium megalosporum	AB120125	82.4	14.9	2.0	0.8
Arthrobotrys oligospora (Aoz1)	AF516146	82.0	12.8	4.0	1.2
Monacrosporium cystosporum	AY859780	85.3	11.8	2.5	0.4
Mutinus elegans	AY859781	82.4	13.9	2.9	0.8
Arthrobotrys conoides	AY859782	85.0	13.4	1.2	0.4
Dactylellina varietas	DQ531603	82.7	13.6	2.5	1.2
Arthrobotrys multisecundaria	EF055263	85.4	12.1	1.7	0.8
Arthrobotrys musiformis	EF113088	83.6	12.3	3.3	0.8
Arthrobotrys yunnanensis	EF113089	85.1	12.0	2.5	0.4
Monacrosporium psychrophilum	EF113090	86.0	13.2	0.4	0.4
Monacrosporium coelobrochum	EF113091	81.6	15.5	1.7	1.3
Dactylella shizishanna	EF113092	85.2	11.5	2.5	0.8
Monacrosporium haptotylum	EF681769	82.4	15.9	0.8	0.8
A. oligospora (PII)	X94121	84.8	13.6	1.2	0.4

All 18 structures showed the common α/β scaffold folding feature of the subtilisin-like serine proteases. Visualization of the superimposed structural models (**Fig. 3**) revealed that the major secondary structure elements were well matched but that some turns and loops, especially those located on the protein surface, showed large structural deviations. This is not surprising, because the secondary structure elements are better conserved and have fewer amino acid insertions and deletions than the loop/turn regions as shown in Supplemental Fig. S1. **Figure 4** shows the molecular surface of Ver112 with color coding for residue variability deduced from these 18 protease sequences. It is apparent that the substrate-binding regions have the lowest residue variability but that the molecular surfaces distant from the active site show relatively high residue variability, with those located opposite the active site exhibiting the highest residue variability, as indicated by the molecular surface representation located on the right side of Fig. 4.

Disulfide bridges contribute to molecular stability

The multiple sequence alignment of the selected 29 proteases revealed several conserved cysteines (Supplemental Fig. S1). Among alkaline proteases, there are 5 absolutely conserved cysteines, of which 4 cysteines form 2 disulfide bridges, Cys156-Cys249(+3) (EF055263 numbering with gaps in AB120125 numbered+1, +2, *etc.*) and Cys302-Cys376, whereas the cysteine at position 201 is free but shared among 27 of the 29 proteases. Interestingly, within the neutral proteases there is another cysteine occupying position 353. However, these 2 cysteines,

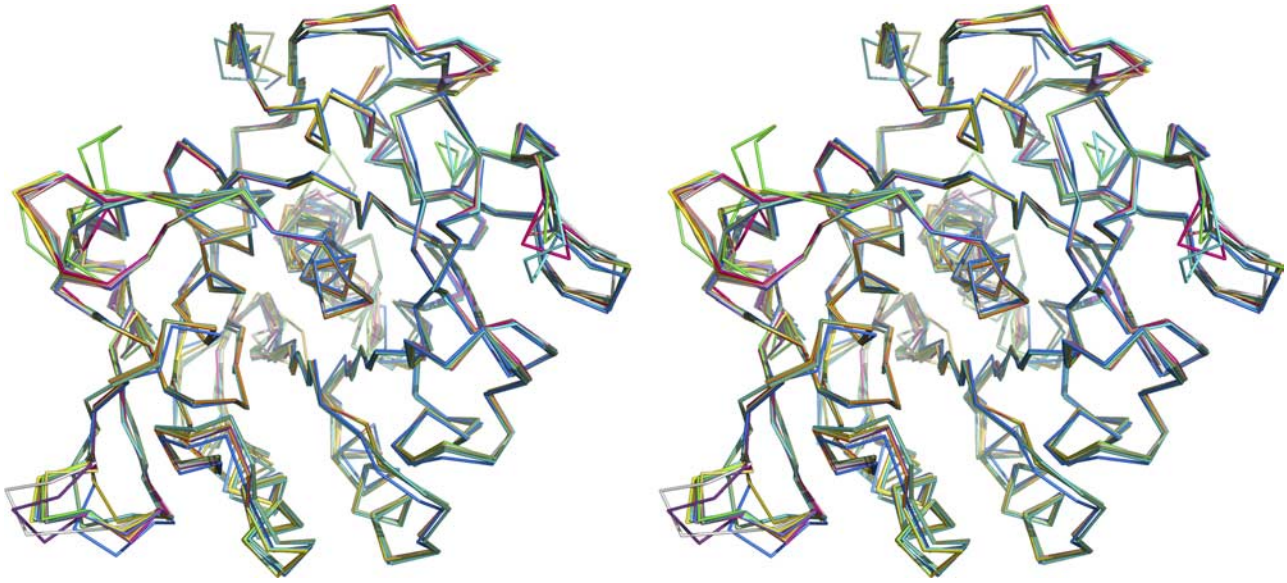

Figure 3. Stereo view of superposition of crystal structures and homologous models of cuticle-degrading proteases. Different structures are drawn with different colors.

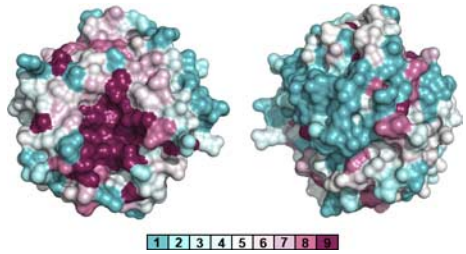

Figure 4. Molecular surface of Ver112. Colors represent residues with different conservation level among cuticle-degrading proteases secreted by nematophagous fungi. Blue is the lowest conservation; grape is the most conservation. Graphic representation was prepared by Consurf Server (http://consurf.tau.ac.il/; ref. 36).

Cys201 and Cys353, cannot form a disulfide bridge due to the large distance separating their side chains (Supplemental Fig. S2). Thus, the alkaline proteases from nematode/insect-parasitic fungi contain 2 disulfide bridges, whereas the neutral proteases from nematode-trapping fungi have no disulfide bridge.

It has been shown that disulfide bridges can contribute to the stability of global or local conformation of a protein (27, 28). To assess the effect of disulfide bridges on structural stability of cuticle-degrading proteases, MD simulations were performed on the wild-type Ver112 and its mutants Ver112_C124A, Ver112_C179A, and Ver112_C124_179A and PII at the condition temperatures of 300 and 400 K, respectively.

To elucidate whether the disulfide bridges contribute significantly to the local stability of the enzyme structure, residues within 5 Å of the center of mass of the 2 disulfide bridges were selected, and the geometrical properties of these selected residues were calculated along the simulation trajectories, respectively (**Table 2**). The residues surrounding the disulfide bridge Cys35-Cys124 were denoted as SS1_5 and those surrounding Cys179-Cys250 were denoted as SS2_5. When the disulfide bridge Cys35-Cys124 was broken, for residue group SS1_5, the average values of the number of natural contacts (NNC) decreased from 5889 to 5774; solvent accessible surface area (SASA) increased from 1113.9 to 1232.4 $Å^2$; and root mean square fluctuation (RMSF) increased from 0.48 to 0.56 Å. On disruption of the disulfide bridge Cys179-Cys250, for residue group SS2_5, the averages of NNC decreased from 6473 to 6417; SASA increased from 897.8 to 927.9 $Å^2$; and the RMSF did not change much. When both disulfide bridges were broken, for both SS1_5 and SS2_5, the average values of their SASA and RMSF increased significantly and the NNC decreased significantly. These statistical results indicate that the disulfide bridges make a substantial contribution to the stabilization of the local structures around the disulfide bridges.

For the mutants Ver112_C124A, Ver112_C179A, and Ver112_C124_179A, the average values of their total SASA and NNC are similar to each other and to those of the wild-type Ver112 during simulations at the temperature 300 K. However, when simulations were performed at 400 K, the average values of the number of hydrogen bonds (NHB), SASA, and NNC for the 3 mutants changed with different amplitude when compared to those for the wild-type protease. These results suggest that the 2 disulfide bridges can also contribute to the global stabilization of molecular structure when the temperature was increased. Our conclusion based on MD simulations that disulfide bridges are important for structural stability of serine protease Ver112 is in agreement with the experimental data obtained from site-directed mutagenesis study on another S8 family protease, Aqualysin I (whose sequence identity to Ver112 is 47%), exhibiting that the disruption of the equivalent disulfide bonds decreased to a large extent the thermal stability of this enzyme (29).

For the 10 ns MD trajectories of PII at temperatures of 300 and 400 K, only the trajectory segments of 4 ns (2–6 ns at 300 K and 4–8 ns at 400 K) seemed able to reach equilibrium due to their stable fluctuation of root mean square deviation curve (Supplemental Fig. S3); therefore, these 2 4-ns trajectories were used for calculation of the geometrical properties of PII. Comparison of C_α RMSF calculated over the trajectories at 300 K between Ver112 and PII (**Fig. 5**) revealed that most residues had higher RMSF in PII than in Ver112. This was further reflected by a higher average RMSF value of PII (0.80 Å) in comparison to Ver112 (0.68 Å). In addition, PII had fewer interatomic contacts (NHB and NNC) and larger SASA than Ver112 (Table 2). Taken together, these structural properties suggest that PII has higher flexibility and is less compact than Ver112. This can be attributed to the lack of equivalent disulfide bridges in PII. However, the overall structure of PII appears to be stable even at 400 K because of similar geometrical properties found between simulations at 300 and 400 K. We considered that, therefore, the disulfide bridge might not be indispensable for the stability of the enzyme structure, while other factors, such as hydrogen bonds and van der Waals contacts, can contribute to the stability of the molecule. For example, for the local conformations of SS1_5 and SS2_5, more NHB and NNC were observed in PII than in Ver112 at 300 K, thus guaranteeing the stability of these local structures in PII.

Disulfide bridges can increase flexibility of substrate-binding site

S1 and S4 substrate-binding pockets are large and have been considered as the primary determinants for substrate specificity and affinity (12, 30). The S1 pocket (S1P) consists of residues 133–136, 159–163, and 223–227 (Ver112 numbering); and the S4 pocket (S4P) is composed of residues 101–105, 108, 133–137, and 142 (Ver112 numbering). To evaluate the change in flexibility of these 2 pockets, average RMSF values of the pocket-residues were calculated and compared either with or without the 2 disulfide bridges (Table 2). On disruption of the disulfide bridge Cys35-Cys124 (Ver112_C124A in Table 2), RMSF of S1P decreased with respect to its starting value (from

TABLE 2. *Comparison of the geometrical properties of PII, Ver112, and Ver112 mutants*

Molecule and simulation temperature	NHB[a]			SASA (Å^2)		
	Total	SS1_5[c]	SS2_5[d]	Total	SS1_5	SS2_5
Ver112, 300 K	212 ± 7	5.054 ± 1.055	7.630 ± 1.481	15,227.0 ± 297.0	1113.9 ± 76.3	897.8 ± 76.9
Ver112_C124A, 300 K	213 ± 7	6.141 ± 1.103	7.814 ± 1.406	15,249.1 ± 279.5	1232.4 ± 72.6	848.8 ± 70.8
Ver112_C179A, 300 K	212 ± 7	5.161 ± 1.155	7.505 ± 1.455	15,253.3 ± 326.8	1093.0 ± 71.2	927.9 ± 79.9
Ver112_C124_179A, 300 K	212 ± 7	5.153 ± 1.234	7.861 ± 1.624	15,243.6 ± 289.9	1202.7 ± 82.8	959.4 ± 87.0
PII, 300 K	210 ± 7	8.308 ± 1.609	13.480 ± 1.572	15,843.3 ± 310.9	1026.8 ± 82.8	1121.4 ± 94.3
Ver112, 400 K	192 ± 9	5.850 ± 1.507	8.343 ± 1.653	16,113.1 ± 397.3	1120.4 ± 84.5	959.4 ± 94.0
Ver112_C124A, 400 K	187 ± 9	4.862 ± 1.332	9.879 ± 1.744	16,137.4 ± 356.2	1118.4 ± 90.4	953.0 ± 85.7
Ver112_C179A, 400 K	186 ± 9	6.142 ± 1.374	6.274 ± 1.421	18,788.4 ± 771.4	1116.3 ± 85.8	967.9 ± 99.5
Ver112_C124179A, 400 K	192 ± 9	4.972 ± 1.514	8.769 ± 1.482	16,761.0 ± 375.2	1285.8 ± 90.9	962.4 ± 92.8
PII, 400 K	192 ± 9	6.894 ± 1.996	11.442 ± 2.093	16,301.2 ± 386.7	1025.5 ± 94.5	1177.4 ± 97.1

0.52 to 0.41 Å) by 21.2%, while RMSF of S4P showed almost no change (0.86 *vs.* 0.87 Å), suggesting that breaking the first disulfide bridge could influence the flexibility of the substrate-binding pocket. The relatively large decrease in flexibility of both the S1 and S4 pockets was observed when the second disulfide bridge, Cys179-Cys250, was disrupted, and the most pronounced effect was observed when both disulfide bridges were disrupted. The reduction in flexibility of substrate-binding pockets on disruption of the disulfide bridge was further reflected by comparison of RMSF between Ver112 and its mutants, as shown in **Fig. 6**. When disulfide bridge Cys35-Cys124 was broken, RMSF values of residues 162, 163, and 223–226 within the S1 pocket and of residues 101, 102, 133, 134, and 142 within the S4 pocket were reduced, although those of residues 103 and 104 in the S4 pocket were increased, resulting in decreased mean RMSF values of both S1 and S4 (Table 2). When disulfide bridge Cys179-Cys250 was broken, RMSF values of residues 133, 160–163, and 223–227 within the S1 pocket and 101–102, 104–105, 133, 137, and 142 within S4 pocket were reduced, while those of residues 134–136 and 159 within the S1 pocket and 103 and 134–136 within the S4 pocket were increased, resulting in reduction in mean RMSF values of both S1 and S4 (Table 2). When both disulfide bridges were broken, RMSF values of most residues located within the S1 and S4 pockets decreased (Table 2).

Correlation between electrostatic surface potential and phylogenetic relationship

The electrostatic surface potentials of the 19 cuticle-degrading proteases were calculated with the Poisson-Boltzmann method using Swiss-PdbViewer (31), and the phylogenetic tree of these proteases was constructed using the NJ method, as described in Materials and Methods. Subtilisin BPN′ and subtilisin Carlsberg were used as outgroups. When placing the electrostatic surface potential representations of these proteases at the corresponding positions of each branch in the phylogenetic tree (**Fig. 7**), good qualitative correlation was found between electrostatic potential and phylogenetic relationship of these proteins. Typically, phylogenetically more similar proteases also have more similar distribution of electrostatic surface potentials. For example, the PII and Aoz1 are located in the same clade and show similarly dense distribution of negatively charged electrostatic potential on protein surfaces (red in Fig. 7). In addition, most proteases within the clade possessing trap devices have a predominant distribution of electronegative potential either on the front surface (except for EF113092 and DQ531603 located in the same branch) or on the backside surface (except for EF113092 and DQ531603 located in the same branch and AB120125 and EF681769 in the same branch). On the contrary, the proteases within the clade possessing no trap device display electronegative character only around the surface of active-site cleft (red in Fig. 7), while other regions of the front surface are largely electroneutral (white in Fig. 7) and the backside surface regions are predominantly electropositive (blue in Fig. 7). It has been shown that the negative charges of the active site could increase its local conformational flexibility, thereby facilitating substrate binding to enzyme (12). This may explain the maintenance of electronegative potential around the active-site cleft surface of these proteases, especially around that of the alkaline cuticle-degrading proteases. On the other hand, previous studies (32–35) have shown that the cuticles of many nematodes are heavily negatively charged and cannot be neutralized easily. We speculate, therefore, that the extracellular alkaline proteases could diffuse preferentially toward nematode cuticle due to the electrostatic attraction between their abundantly positively charged molecular surfaces and the negatively charged nematode cuticle, thereby leading to efficient adhesion to and subsequent degradation of nematode cuticle by alkaline proteases. With regard to the neutral proteases secreted by fungi

TABLE 2. *(continued)*

NNC[b]			C_α RMSF (Å)				
Total	SS1_5	SS2_5	All	SS1_5	SS2_5	S1P[e]	S4P[f]
132,831 ± 742	5889 ± 168	6473 ± 123	0.68 ± 0.29	0.48 ± 0.17	0.41 ± 0.16	0.52 ± 0.14	0.87 ± 0.27
133,114 ± 714	5774 ± 189	6529 ± 144	0.67 ± 0.29	0.56 ± 0.17	0.39 ± 0.13	0.41 ± 0.18	0.86 ± 0.29
132,964 ± 1024	5946 ± 175	6417 ± 137	0.64 ± 0.26	0.49 ± 0.12	0.40 ± 0.09	0.46 ± 0.14	0.72 ± 0.20
133,167 ± 745	5807 ± 181	6307 ± 160	0.68 ± 0.33	0.67 ± 0.26	0.54 ± 0.27	0.36 ± 0.09	0.80 ± 0.28
130,681 ± 758	6959 ± 163	6572 ± 112	0.80 ± 0.41	0.64 ± 0.18	0.56 ± 0.20	0.42 ± 0.09	0.91 ± 0.29
129,714 ± 1359	5906 ± 217	6354 ± 158	1.57 ± 0.85	0.80 ± 0.28	0.84 ± 0.58	1.17 ± 0.48	1.57 ± 0.49
129,908 ± 1154	5890 ± 220	6250 ± 221	1.51 ± 0.78	0.92 ± 0.27	0.84 ± 0.29	1.33 ± 0.35	2.21 ± 0.45
130,214 ± 1136	6177 ± 261	6202 ± 194	1.38 ± 0.65	0.80 ± 0.30	0.83 ± 0.41	1.37 ± 0.55	1.02 ± 0.33
129,795 ± 1057	5742 ± 265	6424 ± 219	1.45 ± 0.76	1.28 ± 0.52	0.83 ± 0.39	0.82 ± 0.18	1.73 ± 0.46
130,129 ± 1200	6764 ± 266	6385 ± 148	1.58 ± 0.62	1.23 ± 0.44	0.99 ± 0.31	0.92 ± 0.28	1.62 ± 0.34

NHB, number of hydrogen bonds; SASA, solvent accessible surface area; NNC, number of native contacts; RMSF, root mean square fluctuation. [a]A hydrogen bond is considered to exist when the donor-hydrogen-acceptor angle is >120° and the donor-acceptor distance is <3.5 Å. [b]A native contact is considered to exist if the distance between 2 atoms is <6 Å. [c]Residues within 5 Å of the center of mass of the disulfide bridge Cys35-Cys124. [d]Residues within 5 Å of the center of mass of the disulfide bridge Cys179-Cys250. [e]S1 pocket. [f]S4 pocket.

that have trapping devices, their diffusion toward nematode cuticle seems to be suppressed due to the electrostatic repulsion between the heavily negatively charged proteases and the negatively charged cuticle. However, such repulsion is unlikely to have a significant effect on this group of fungi, because their trap devices can actively capture the nematode, thus facilitating the contact between the host and the proteases, leading to effective degradation of the nematode cuticle.

CONCLUSION

Phylogenetic analysis combined with a comparison of electrostatic surface potential suggests that the 19 cuticle-degrading proteases can be divided into 2 main groups: alkaline proteases from parasitic fungi and neutral proteases from nematode-trapping fungi. These proteases share a relatively high degree of sequence identity and have very similar molecular structure. Notably, they also play a similar role in degrading host cuticle during fungal infection of nematodes. Nevertheless, the subtle differences in amino acid components of substrate-binding regions and other regions, such as loops and turns, can result in differences in the architecture of substrate-binding pockets and other structural regions, leading to changes in their physicochemical properties, such as optimal reaction temperature, thermal stability, and electrostatic surface potential of these proteases. Disulfide bridges were only observed in alkaline protease, which contributes to the stabilization of the local/global structures and, interestingly, enhances the structural flexibility of the substrate pockets S1 and S4. This may explain why the alkaline proteases have higher substrate affinity and catalytic activity than neutral proteases, as indicated by their relatively higher nematicidal activities in comparison to neutral proteases. The nematode-trapping fungi can capture nematodes effectively using their trapping devices; subsequently, the secreted neutral proteases degrade the trap-captured nematode "unhurriedly," thus

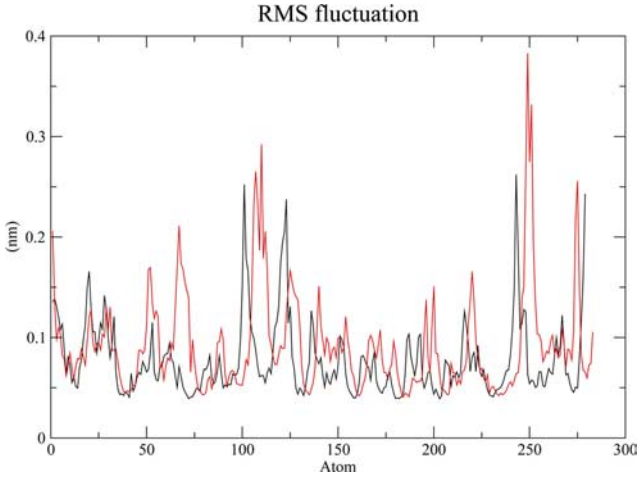

Figure 5. C_α RMSF of Ver112 (black) and PII (red) as a function of residue number. RMSF values were calculated over MD trajectories at 300 K.

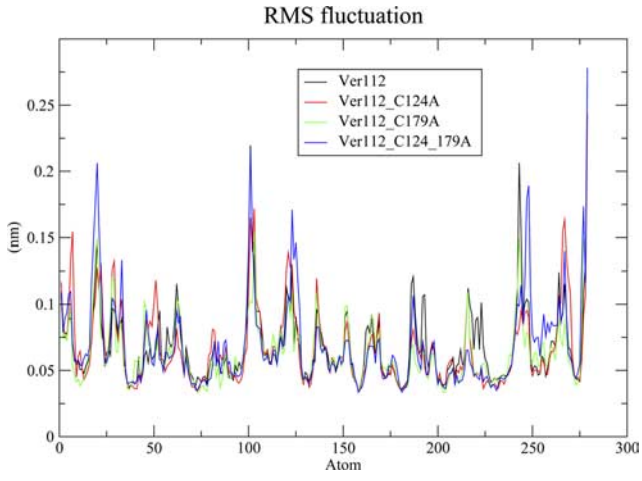

Figure 6. Comparison between RMSF values of Ver112 and its mutants. RMSF curves were calculated over MD trajectories at 300 K and are shown in different colors, as indicated.

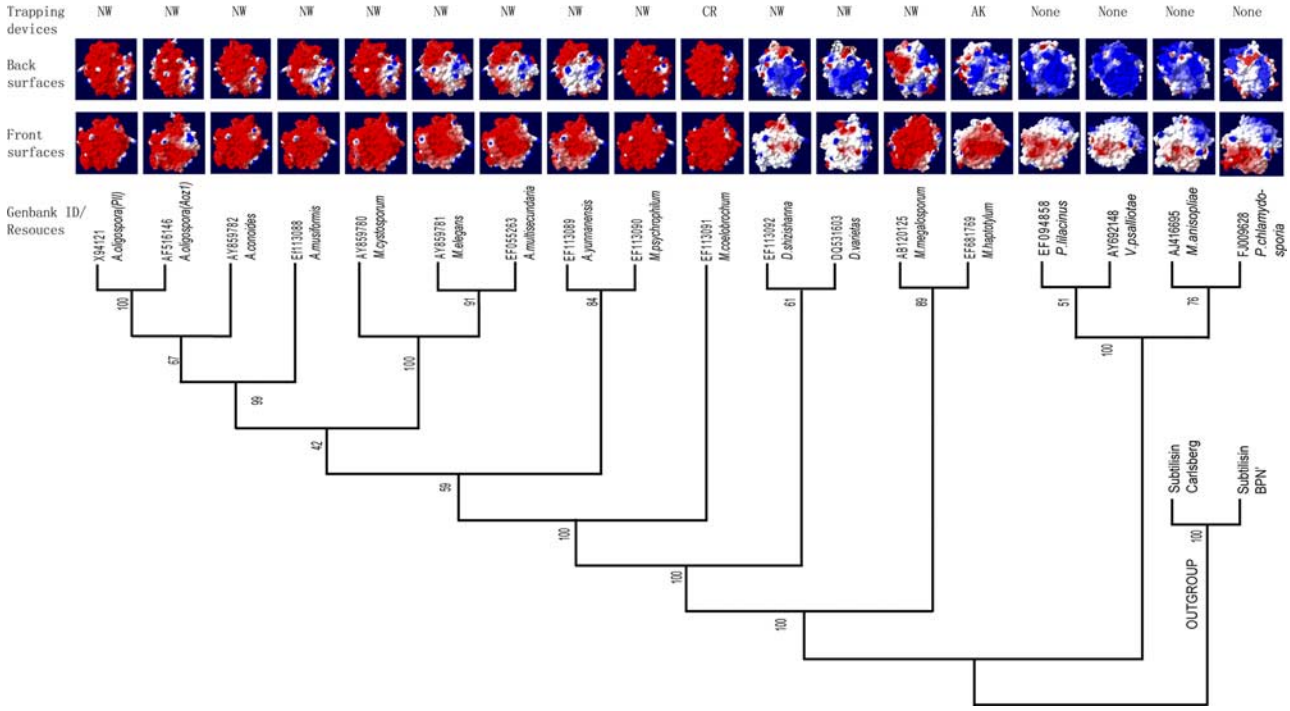

Figure 7. Arrangement of molecular electrostatic potential surfaces of proteases along with their NJ phylogenetic tree. Front surfaces were defined as surfaces containing active site at the center; back surfaces are opposite to front surfaces. Trapping devices are as follows: NW, networks; CR, constricting rings; AK, adhesive knobs; none, no trapping devices.

eliminating the constraints faced by non-nematode-trapping/nematode-parasitic fungi. We conclude that, with the aid of trapping devices, the neutral cuticle-degrading proteases may be subjected to a low selective pressure, whereas nematode-parasitic fungi do not have trapping devices, and therefore their alkaline protease has evolved to be more powerful to kill nematodes as rapidly as possible (11). FJ

The authors thank Dr. Jianping Xu (McMaster University, Hamilton, ON, Canada) for help and advice in this experiment and the High Performance Computer Center of Yunnan University for computational support. This work was jointly funded by the National Basic Research Program of China (approval 2007CB411600); projects from the National Natural Science Foundation of China (approvals 30630003, 30860011, 30960229, and 30660107); the Department of Science and Technology of Yunnan Province (approvals 2007PY-22, 2007C007Z, and 2009CI052); the Yunnan Branch of China Tobacco Industrial Corporation (grant 2010YN17); and Yunnan University (grant 2010C02Z).

REFERENCES

1. Yang, J. K., Tian, B. Y., Liang, L. M., and Zhang, K. Q. (2007) Extracellular enzymes and the pathogenesis of nematophagous fungi. *Appl. Microbiol. Biotechnol.* **75,** 21–31
2. Tunlid, A., Rosen, S., Ek, B., and Rask, L. (1994) Purification and characterization of an extracellular serine protease from the nematode-trapping fungus *Arthrobotrys oligospora*. *Microbiology* **140,** 1687–1695
3. Zhao, M. L., Mo, M. H., and Zhang, K. Q. (2004) Characterization of a neutral serine protease and its full-length cDNA from the nematode-trapping fungus *Arthrobotrys oligospora*. *Mycologia* **96,** 16–22
4. Segers, R., Butt, T., Kerry, B., and Peberdy, J. (1994) The nematophagous fungus *Verticillium chlamydosporium* produces a chymoelastase-like protease which hydrolyses host nematode proteins in situ. *Microbiology* **140,** 2715–2723
5. Joshi, L., St Leger, R. J., and Bidochka, M. J. (1995) Cloning of a cuticle-degrading protease from the entomopathogenic fungus, *Beauveria bassiana*. *FEMS Microbiol. Lett.* **125,** 211–217
6. St Leger, R., Charnley, A., and Cooper, R. (1987) Characterization of cuticle-degrading proteases produced by the entomopathogen *Metarhizium anisopliae*. *Arch. Biochem. Biophys.* **253,** 221–232
7. Åhman, J., Johansson, T., Olsson, M., Punt, P. J., van den Hondel, C. A., and Tunlid, A. (2002) Improving the pathogenicity of a nematode-trapping fungus by genetic engineering of a subtilisin with nematotoxic activity. *Appl. Environ. Microbiol.* **68,** 3408–3415
8. Morton, C. O., Hirsch, P. R., Peberdy, J. P., and Kerry, B. R. (2003) Cloning of and genetic variation in protease VCP1 from the nematophagous fungus *Pochonia chlamydosporia*. *Mycol. Res.* **107,** 38–46
9. Liang, L. M., Meng, Z. H., Ye, F. P., Yang, J. K., Liu, S. Q., Sun, Y. N., Guo, Y., Mi, Q. L., Huang, X. W., Zou, C. G., Rao, Z. H., Lou, Z. Y., and Zhang, K. Q. (2010) The crystal structures of two cuticle-degrading proteases from nematophagous fungi and their contribution to infection against nematodes. *FASEB J.* **24,** 1391–1400
10. Huang, X. W., Zhao, N. H., and Zhang, K. Q. (2004) Extracellular enzymes serving as virulence factors in nematophagous fungi involved in infection of the host. *Res. Microbiol.* **155,** 811–816
11. Li, J., Yu, L., Yang, J. K., Dong, L. Q., Tian, B. Y., Yu, Z. F., Liang, L. M., Zhang, Y., Wang, X., and Zhang, K. (2010) New insights into the evolution of subtilisin-like serine protease genes in *Pezizomycotina*. *BMC Evol. Biol.* **10,** 68
12. Liu, S. Q., Meng, Z. H., Yang, J. K., Fu, Y. X., and Zhang, K. Q. (2007) Characterizing structural features of cuticle-degrading proteases from fungi by molecular modeling. *BMC Struct. Biol.* **7,** 33
13. Yang, J. K., Huang, X. W., Tian, B. Y., Wang, M., Niu, Q. H., and Zhang, K. Q. (2005) Isolation and characterization of a serine protease from the nematophagous fungus, *Lecanicillium psalliotae*, displaying nematicidal activity. *Biotechnol. Lett.* **27,** 1123–1128

14. Dong, L. Q., Mo, M. H., Yang, J. K., and Zhang, K. Q. (2007) A method for obtaining quantities of *Caenorhabditis elegans* eggs. *Nematology* **9,** 743–744(742)
15. Larkin, M. A., Blackshields, G., Brown, N. P., Chenna, R., McGettigan, P. A., McWilliam, H., Valentin, F., Wallace, I. M., Wilm, A., Lopez, R., Thompson, J. D., Gibson, T. J., and Higgins, D. G. (2007) Clustal W and Clustal X version 2.0. *Bioinformatics* **23,** 2947–2948
16. Tamura, K., Dudley, J., Nei, M., and Kumar, S. (2007) MEGA4: molecular evolutionary genetics analysis (MEGA) software version 4.0. *Mol. Biol. Evol.* **24,** 1596–1599
17. Sali, A., and Blundell, T. L. (1993) Comparative protein modelling by satisfaction of spatial restraints. *J. Mol. Biol.* **234,** 779–815
18. Hess, B., Kutzner, C., van der Spoel, D., and Lindahl, E. (2008) GROMACS 4: Algorithms for highly efficient, load-balanced, and scalable molecular simulation. *J. Chem. Theory Comput.* **4,** 435–447
19. Lindahl, E., Hess, B., and van der Spoel, D. (2001) GROMACS 3.0: a package for molecular simulation and trajectory analysis. *J. Mol. Model.* **7,** 306–317
20. Laskowski, R. A., MacArthur, M. W., Moss, D. S., and Thornton, J. M. (1993) PROCHECK: a program to check the stereochemical quality of protein structures. *J. Appl. Crystallogr.* **26,** 283–291
21. Berendsen, H. J. C., Postma, J. P. M., van Gunsteren, W. F., and Hermans, J. (1981) Interaction models for water in relation to protein hydration. In *Intermolecular Forces* (Pullman, B., ed) pp. 331–342, Reidel, Dordrecht, The Netherlands
22. Berendsen, H. J. C., Postma, J. P. M., Vangunsteren, W. F., Dinola, A., and Haak, J. R. (1984) Molecular-dynamics with coupling to an external bath. *J. Chem. Phys.* **81,** 3684–3690
23. Tironi, I., Sperb, R. E., Smith, P., and van Gunsteren, W. (1995) A generalized reaction field method for molecular dynamics simulations. *J. Chem. Phys.* **102,** 5451–5459
24. Hess, B., Bekker, H., Berendsen, H., and Fraaije, J. (1997) LINCS: A linear constraint solver for molecular simulations. *J. Comput. Chem.* **18,** 1463–1472
25. Li, J., Yang, J. K., Huang, X. W., and Zhang, K.-Q. (2006) Purification and characterization of an extracellular serine protease from *Clonostachys rosea* and its potential as a pathogenic factor. *Process Biochem.* **41,** 925–929
26. Liu, S. Q., Meng, Z. H., Fu, Y. X., and Zhang, K. Q. (2010) Insights derived from molecular dynamics simulation into the molecular motions of serine protease proteinase K. *J. Mol. Model.* **16,** 17–28
27. Fersht, A., and Serrano, L. (1993) Principles of protein stability derived from protein engineering experiments. *Curr. Opin. Struc. Biol.* **3,** 75–83
28. Matsumura, M., Signor, G., and Matthews, B. W. (1989) Substantial increase of protein stability by multiple disulphide bonds. *Nature* **342,** 291–293
29. Sakaguchi, M., Takezawa, M., Nakazawa, R., Nozawa, K., Kusakawa, T., Nagasawa, T., Sugahara, Y., and Kawakita, M. (2008) Role of disulphide bonds in a thermophilic serine protease aqualysin I from *Thermus aquaticus* YT-1. *J. Biochem.* **143,** 625–632
30. Tao, Y., Rao, Z. H., and Liu, S. Q. (2010) Insight derived from molecular dynamics simulation into substrate-induced changes in protein motions of proteinase K. *J. Biomol. Struct. Dyn.* **28,** 143–158
31. Guex, N., and Peitsch, M. C. (1997) Swiss-Model and the Swiss-PdbViewer: an environment for comparative protein modeling. *Electrophoresis* **18,** 2714–2723
32. Blaxter, M. L., Page, A. P., Rudin, W., and Maizels, R. M. (1992) Nematode surface coats: actively evading immunity. *Parasitol. Today* **8,** 243–247
33. Cox, G., Kusch, M., and Edgar, R. (1981) Cuticle of *Caenorhabditis elegans*: its isolation and partial characterization. *J. Cell Biol.* **90,** 7–17
34. Himmelhoch, S., and Zuckerman, B. M. (1978) *Caenorhabditis briggsae:* aging and the structural turnover of the outer cuticle surface and the intestine. *Exp. Parasitol.* **45,** 208–214
35. Murrell, K. D., Graham, C. E., and McGreevy, M. (1983) *Strongyloides ratti* and *Trichinella spiralis*: net charge of epicuticle. *Exp. Parasitol.* **55,** 331–339
36. Landau, M., Mayrose, I., Rosenberg, Y., Glaser, F., Martz, E., Pupko, T., and Ben-Tal, N. (2005) ConSurf 2005: the projection of evolutionary conservation scores of residues on protein structures. *Nucleic Acids Res.* **33,** W299–W302

Received for publication October 26, 2010.
Accepted for publication February 10, 2011.